Dalton Transactions

Accepted Manuscript

ROYAL SOCIETY OF CHEMISTRY

www.rsc.org/dalton

Cite this: DOI: 10.1039/c0xx00000x

www.rsc.org/xxxxxx

Article

Carbon coating stabilized Ti^{3+}-doped TiO_2 for photocatalytic hydrogen generation under visible light irradiation

Gao Fu,[a] Peng Zhou,[a] Meiming Zhao,[b] Weidong Zhu,[a] Shicheng Yan*[,b,c,d], Tao Yu*[a,c,d] and Zhigang Zou[a,b,c,d]

Received (in XXX, XXX) Xth XXXXXXXXX 20XX, Accepted Xth XXXXXXXXX 20XX
DOI: 10.1039/b000000x

Abstract: Self doping by Ti^{3+} is a useful way to expand the light response of TiO_2 into visible light region. However, to obtain a stable Ti^{3+}-doped TiO_2 seems a challenge due to the easy oxidation of Ti^{3+} during the heterogeneous reaction. Here, we proposed a simple carbon coating route to stabilize the Ti^{3+}-doped TiO_2, in which both the Ti^{3+} and precursor of carbon coating layer were in situ formed from the hydrothermal hydrolysis of titanium isopropoxide. The carbon coated Ti^{3+}-doped TiO_2 exhibited the excellent stability for photocatalytic hydrogen production. Based on electron paramagnetic resonance (EPR) analysis, a proposed stabilizing mechanism is that the conductive carbon coating layer as a barrier layer prevents the H_2O and O_2 from diffusing into the surface of the photocatalyst, which can oxidize the surface O vacancies and Ti^{3+} in TiO_2. Our findings offer a simple route to preparing the highly stable TiO_2-based photocatalyst with visible light response.

1. Introduction

Since Fujishima discovered that TiO_2 can act as a photo-electrochemical water-splitting catalyst in 1972,[1] which was once proposed as the most promising material for large-scale hydrogen production.[2] However, the large band gap (3.2 eV for anatase and 3.0 eV for rutile) determined that the TiO_2 only absorbed the ultraviolet light which makes up 3.5% of the solar energy, corresponding to a low solar-to-hydrogen conversion efficiency of 1.8%.[2-5] Enormous efforts, such as element doping, organic compounds sensitizing and forming heterojunctions with narrow-band-gap semiconductors were made for expanding light absorption edge of TiO_2.[6, 7] For element doping, self-doping of Ti^{3+} into crystal lattice of TiO_2, which introduced an energy level (0.7-1.2eV) below the conduction band (CB) of TiO_2,[3] could not only red shift the absorption band edge, but also increase the carries concentration.[2] Therefore, Ti^{3+} doping was considered to be an effective and promising route for obtaining the visible-light-response TiO_2-based photocatalysts.[8, 9]

Ti^{3+} could be made from reduction of Ti^{4+} or oxidization of Ti^{2+}.[9] A general method to obtain the Ti^{3+}-doped TiO_2 is using the reducers with strong reductive ability, such as 2-ethylimidazole[10, 11], N_2H_4[12], H_2[13] and $NaBH_4$[14, 15], to reduce Ti^{4+} to Ti^{3+} by calcining or hydrothermal treatment. In these routes reported, the products usually were rutile TiO_2 or a mixture of rutile and anatase TiO_2 due to the facile phase transformation from anatase to rutile during the calcination. A few researches have reported Ti^{3+} doped anatase TiO_2 by a hydrolysis-hydrothermal method, using Ti^{3+} salts as the source of the Ti^{3+}.[16-18] In addition, the Ti^{3+} either on the surface or in the bulk of TiO_2 are usually not stable enough and easily oxidized by H_2O or O_2.[18] Therefore, it seems a challenge to prepare the stable Ti^{3+}-doped TiO_2 with anatase phase. Directly burning the carbon-containing Ti precursor in ethanol, the 200 h photostable Ti^{3+}-doped TiO_2 with a mixture phase of anatase and rutile was prepared. However, there was no explanation on the high stability of Ti^{3+} in such prepared TiO_2. Noting that the elemental analysis proved the existence of the carbon in the sample, this probably means that the surface carbon as a protective layer prevents Ti^{3+} from oxidizing by H_2O and O_2.[10] Indeed, it has been demonstrated that the carbon coating can improve the stability of photocatalysts such as CdS[19] and MnO_x[20], and also can suppress the phase transformation from anatase to rutile at high temperatures.[21, 22] These evidence indicated that the highly stable Ti^{3+}-doped anatase TiO_2 can be prepared by using the carbon coating method to stabilize both the Ti^{3+} and anatase phase.

Here, we used an in situ hydrolysis of titanium isopropoxide to form carbon-coated anatase TiO_2 nanocrystals with Ti^{3+} doping into the crystal lattice. We found that both the bulk Ti^{3+} and surface oxygen vacancies were stable in the carbon coated Ti^{3+}-doped TiO_2 photocatalyst during 12 h photocatalytic hydrogen production. EPR analysis confirmed that the highly stable Ti^{3+} in carbon coated TiO_2 resulted from the protective effect of surface carbon coating layer. Our results provided a simple method to obtain stable Ti^{3+}-doped TiO_2 for applications in the field of photocatalysis.

Experimental details

A slightly improved hydrothermal way with subsequent calcination was used to prepare the carbon coated Ti^{3+}-doped TiO_2 nanocrystals.[23] Firstly, 31 g titanium isopropoxide was added to 6.8 g acetic acid with magnetically stirring for 15 min at

room temperature. After that, the mixture was added drop by drop into 160 mL-vigorous-stirring distilled water. Due to the hydrolysis of titanium isopropoxide, a suspension was made. After stirring for 1 h, 2 mL 65 wt% HNO_3 was added into the suspensions and then were heated at 75 °C for 80 min for obtaining a colloid solution. Then, about 40 mL distilled water was added and the resulting solution was transformed to a 300-mL titanium autoclave and heated at 250 °C for 12 h to obtain the organics coated Ti^{3+}-doped TiO_2 nanocrystals (denoted as sample A). For obtaining a thinner organics coating layer (Fig.S1, ESI†), sample A was washed by 1M NaOH for four times and then by ethanol and distilled water twice separately to partially remove the surface organics (denoted as sample B). Both the two samples were freeze-drying to remove the remained water. Both the samples A and B were calcined at 350 and 550 °C for 4 h with a heating rate of 5 °C/min in Ar for the carbonization of surface organics. According to the heating temperature, the corresponding products were marked as sample A-350, A-550, B-350 and B-550, respectively.

Phases of all the samples were identified by a powder X-ray diffraction (XRD, Ultima III, Rigaku Corp., Japan) using Cu Kα (λ=1.54178 Å, 40 kV, 40 mA) with a scan rate of 10 °/min. The diffuse reflectance spectroscopy were collected using a UV-visible spectrophotometer (Shimadzu Corp., UV-2500PC, Japan). X-ray photoelectron spectroscopy (XPS) was carried out on Thermo ESCALAB 250 spectrometer (Al Kα), and the photoelectrons were detected by a hemispherical analyzer operating at a passive energy of 20 eV. The binding energy was calibrated on the reference C 1s peak at 284.8 eV. The high-resolution transmission electron microscopy (HR-TEM) analysis was conducted using a JEOL 3010 transmission electron microscope. Electron paramagnetic resonance (EPR) measurement was carried out on a Bruker EMX-10/12 EPR spectrometer with a frequency of 9.8485 GHz at the room temperature. The mass-normalized EPR spectra were from the intensity of measured EPR signal dividing the mass of the sample. The qualitative EPR analysis was carried out on a JEOL JES-FA200 spectrometer with a frequency of 9.0615 GHz at 77K. The thermogravimetric-differential scanning calorimetry analysis (TG-DSC) was performed using a thermoanalytical apparatus (STA 449C, NETZSCH) under an air atmosphere at a heating rate of 5 °C/min.

Results and Discussion

The XRD patterns of the samples prepared by hydrothermal treatment with or without sequent calcination were shown in Fig.1a. It could be found that, except for sample B-550, which was a mixture phase of rutile and anatase, all the other samples were anatase (JCPDS No. 21-1272). As the annealing temperature rose, the crystallinity of the samples had no obvious change. This indicated that the crystalline anatase TiO_2 was formed during the hydrothermal treatment. The calcination did not change the phase structure and crystallinity if the heating temperature was below 550 °C. The average sizes of the TiO_2 particles were estimated to be 20-30 nm according to Scherrer's equation, indicating that no obvious change in particle size occurred during the washing and annealing processes (Table S1 of ESI†). It was worth pointing out that the sample A-550 was anatase phase, but the sample B-550 exhibited a mixture phase of rutile (JCPDS No. 21-1276) and anatase. This probably resulted from that surface organics from the hydrolysis of titanium isopropoxide on the sample A suppressed the phase transition to occur, as demonstrated in the previous reports.[21, 24]

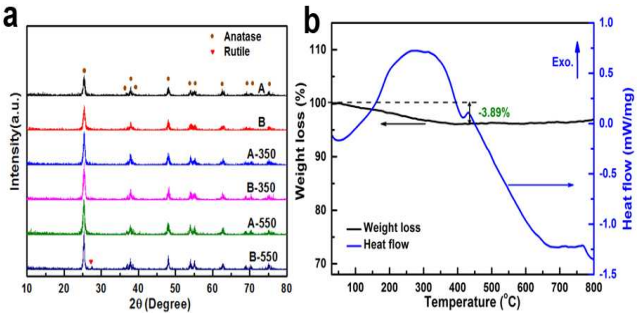

Fig.1 XRD patterns for samples A, A-350, A-550, B, B-350 and B-550 (a). TG-DSC of sample A in air (b).

TG-DSC analysis was performed to understand the thermal stability of sample A and the result was shown in Fig.1b. There was a wide endothermic peak from 200 to 400 °C in the DSC, which could be assigned to the burning of surface organics. A narrow endothermic peak at 420 °C corresponded to the phase transformation from anatase to rutile phase. This evidence meaned that the samples A-350 and B-350 prepared at 350 °C were pure anatase phase and the carbon coating can be formed on the surface by carbonization of surface organics. The samples A-550 and B-550 prepared at the 550 °C, which was much higher than the phase transformation temperature, should be a mixture phase. However, XRD pattern of the sample A-550 did not exhibit obvious rutile phase, probably due to that the content of rutile phase was lower than the XRD detection limitation (5% for volume percentage), resulting from the suppression effect of surface organic layer.[21] Indeed, heating the sample A after partially removing the surface organics by washing would produce a product with a mixture phase (sample B-550). The weight fraction of rutile content in sample B-550 was calculated by the Scherrer's equation of $W_R = I_R/(I_R+0.079I_A)$, where W_A was the weighted fraction of anatase in the mixed phase, and I_A and I_R were the integrated intensity of corresponding anatase (101) and rutile (110) diffraction peaks, respectively.[25] The calculated W_R was 0.1 for sample B-550, confirming that the surface organics can suppress the phase transition compared to the sample A-550.

The TEM observations (Fig.2a and Fig.S2 in ESI†) showed that these samples were 20-30 nm nanocrystals, in good agreement with the XRD calculations. The HR-TEM crystal lattice fringes (Fig.2b-d) of the whole nanocrystal indicated that these as-prepared samples were single crystals. A 2-3 nm-thick amorphous layer was observed on the surface of the sample A-350 (Fig.2b). Increasing the temperature to 550 °C, thickness of the amorphous layer decreased to about 1 nm due to the

decomposition or/and carbonization of organics at high temperature (Fig.2c), as demonstrated in DSC. However, no amorphous layer is visible on the surface of sample B-350 (Fig.2d), which convinced that the surface organics could be washed away by the NaOH solution and ethanol.

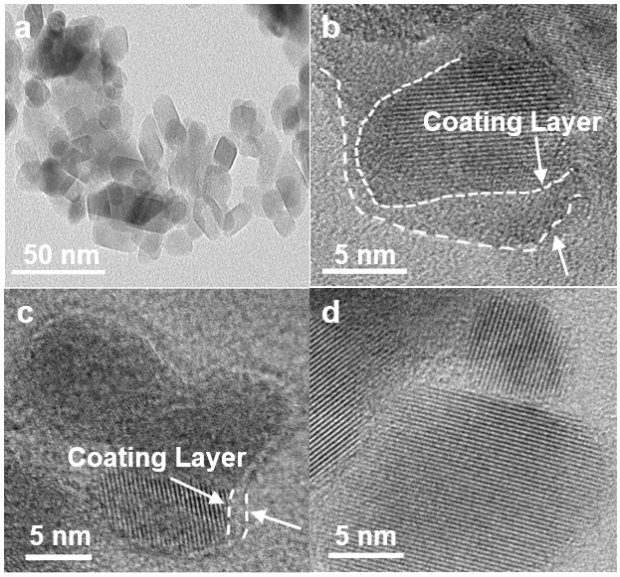

Fig.2 TEM morphology of sample A (a). HR-TEM images for the samples A-350 (b), A-550 (c) and B-350 (d).

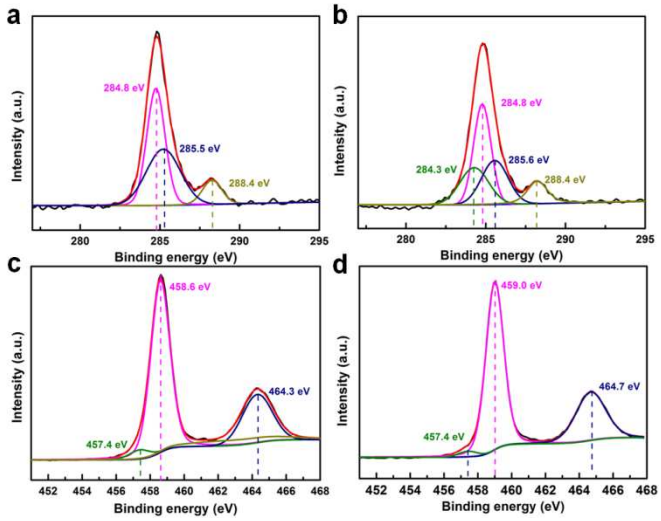

Fig.3 XPS spectra for C 1s and Ti 2p in sample A (a, c) and in sample A-350 (b, d).

XPS measurement was performed for further confirming the surface composition of as-prepared samples. The C 1s XPS spectrum of sample A was shown in Fig.3a and can be divided into three peaks. The peak at 284.8 eV was mainly attributable to amorphous C-C bonding, 285.5 eV to the C-OH and 288.4 eV to -COOH.[26] Although sample B were washed by 1M NaOH, ethanol and distilled water, the XPS spectrum of C 1s (Fig.S1b of ESI†) still showed the existence of C–OH and –COOH, which had been reported that the C–OH and –COOH were strong anchoring groups on the surface of TiO_2,[27-28] and –COOH was much better. These observations implied that the organics existed on the surface of sample A. According to the TG result, the content of surface organics was about 3.89 % of the total mass of TiO_2 nanocrystals. The isopropanol was detected by liquid chromatography during the hydrolysis of titanium isopropoxide, which can be the main source of organics absorbed on the surface of TiO_2. After heating the sample A at 350 °C, the contents of -COOH and C-OH decreased and a new C 1s peak at 284.3 eV appeared and can be assigned to the C=C in the graphitic-phase carbon (Fig.3b),[26] originating from the carbonization of organics. With increasing the heat temperature, the content of graphite-phase carbon increased due to the increase of carbonized degree of organics (Fig.S2, ESI†).

Three peaks were observed in the Ti 2p XPS spectrum of sample A (Fig.3c). Peaks at 458.6 eV and 464.3 eV were Ti^{4+} $2p_{3/2}$ and $2p_{1/2}$. A low-intensity peak at 457.4 eV was assigned to Ti^{3+} $2p_{3/2}$,[33] confirming that the Ti^{3+} formed on the surface of TiO_2 nanocrystals. The content of Ti^{3+} slightly decreased after heating sample A at 350 °C due to its thermal instability (Fig.3d). Sample B-350 exhibited much lower intensity of Ti^{3+} XPS peak than sample A-350 (Fig.S3, ESI†), meaning that the surface organics could partially prevent oxidation of Ti^{3+} during the annealing. However, no peak at 457.4 eV was found when the sample A or B was heated at as high temperature as 550°C (Fig.S2, ESI†), instructing that the surface Ti^{3+} was completely oxidized at such high temperature.[32]

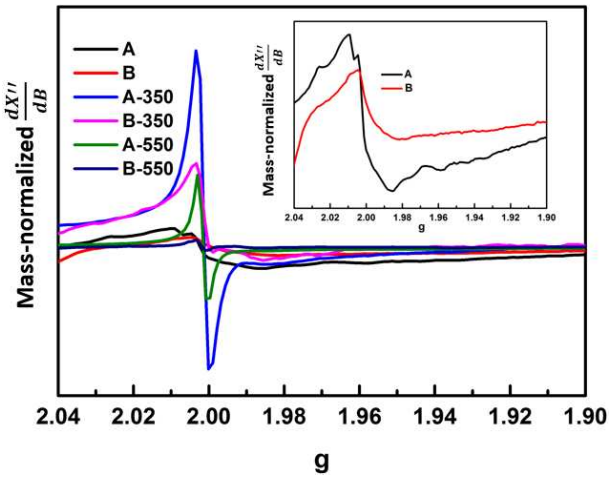

Fig.4 Normalized EPR spectra for A-350, B-350, A-550 and B-550. Inset shows the normalized EPR spectra for samples A and B.

The EPR analysis is a useful tool to distinguish the surface and bulk Ti^{3+}. The observed g values in the sample A were 1.959 and 1.986, corresponding to the $g_{\parallel}$ and $g_{\perp}$ (inset in Fig.4), are a clear indication of Ti^{3+} doping into the bulk of TiO_2 during the hydrothermal reaction.[8] The C-OH in the isopropanol from the hydrolysis of titanium isopropoxide was considered to be a good reducer for reducing Ti^{4+} to Ti^{3+}.[33] In our case, the growth of TiO_2 single crystal was kinetically slow in the presence of acetic acid buffer solution.[32] We believe that the isopropanol reducing Ti^{4+} to Ti^{3+} occurs during the whole growing process of TiO_2 single crystal, thus forming a Ti^{3+} bulk-doped TiO_2. In order to

determine the concentration of Ti^{3+} in the TiO_2 catalyst, the quantified EPR analysis was carried out. A qualitative EPR analysis through double integration of the peak relative to that of a $3d^5$ signal of Mn^{2+}, showed that the concentration of Ti^{3+} was about 0.0033% of all the Ti centers in the TiO_2, which was the comparable level with the reported results.[11] An EPR signal at g=2.026 represented the existence of the surface O_2^-,[10] which suggested that Ti^{3+} also formed on the surface of TiO_2. For the samples A-350, B-350 and A-550, the surface Ti^{3+} signal disappeared due to its thermal instability and a strong EPR signal at g=2.004, assigning to the formation of surface oxygen vacancies.[10] As annealing in the atmosphere without oxygen could generated more oxygen vacancies by eliminating surface oxygen atoms,[8] largely enhancing EPR signal of oxygen vacancies. The locally enlarged observations on Fig. 4 indicated that the signal of bulk Ti^{3+} became weak lightly after the heat treatment (Fig.S7 of ESI†). All the samples calcined at 550 °C showed much weak intensity of Ti^{3+} in the bulk, due to that the Ti^{3+} was very sensitive to heating. Sample A-350 shows much higher intensity of oxygen vacancies on the surface and Ti^{3+} in the bulk than sample A-550, indicating that at higher temperature surface oxygen vacancies can be oxidized by oxygen-containing organics and the bulk Ti^{3+} transformed to Ti^{4+} by losing the excess electron that was withdrawn by interstitial or surface oxygen adatoms.[36]

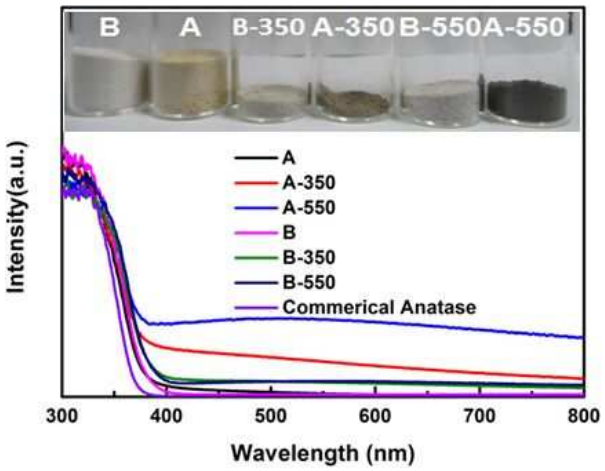

Fig 5. UV-Vis absorption spectra of the as-prepared samples A, B, A-350, B-350, A-550 and B-550. For comparison, UV-Vis spectrum of the commercial anatase TiO_2 was also shown here.

The optical properties for these as-prepared samples were checked by UV-Vis spectrophotometer, as shown in Fig.5. The absorption spectra for all the samples shifted to a longer wavelength revealing a decrease in the band gap. Meanwhile, the absorbance in the visible range was enhanced, compared to the stoichiometric anatase. This phenomenon was consistent with the theoretical calculation, owing to that an electronic band from Ti^{3+} doping was located just below the conduction band of pure TiO_2. It was obvious that these as-prepared samples exhibited significant differences in the background absorption. With increasing the heat temperature, the background absorption of both the sample A and B increased due to the increase of carbonized degree of surface organics. The gradual increasing color of samples (inset of Fig.5) further confirmed that the content increase of graphite-phase carbon with increasing the heat temperature, which would induce the strong background absorption. The content of graphite-phase carbon on sample B-350 or B-550 was obviously lower than that on the sample A-350 or A-550, confirming that the surface organics on Ti^{3+}-doped TiO_2 indeed can be partially removed by chemical washing.

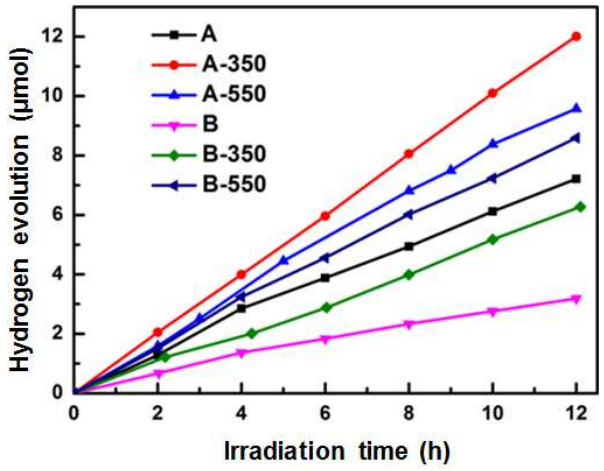

Fig.6 Photocatalytic hydrogen generation over the carbon coated Ti^{3+}-doped TiO_2 under irradiation of visible light (λ≥420 nm).

The photocatalytic hydrogen production was performed by dispersing 0.1 g catalyst in a mixture solution of 220 mL distilled water and 50 mL CH_3OH. 0.5wt% Pt co-catalyst was loaded onto the surface of the Ti^{3+}-doped TiO_2 by photo-deposition method under the full arc irradiation of Xe lamp for 2 h.[33] As shown in Fig.6, sample A-350 showed the highest and most stable activity of hydrogen production with a slope of 1 μmol/h, within the 12 h visible light irradiation (Fig.S4 of ESI†). Sample A, A-550, B, B-350 and B-550 got the slopes of 0.6, 0.75, 0.4, 0.6 and 0.7 μmol/h respectively in the first 2 h, but they all suffered a gradually decreased activity during the sequential 10 h. Due to the coexistence of rutile and anatase phase, sample B-550 exhibited a better photo-activity than sample B and B-350, probably resulting from the improved charge separation efficiency by heterojunction effect.[42,43] Except for sample B-550, all the samples with carbon coating layers showed better activity in hydrogen generation than those without carbon coating layers under the visible light irradiation. Sample A-350 contained 2.1wt% carbon on the surface, which was determined by TG (Fig.S6 of ESI†), showed the best activity and stability of utilizing visible light of generating hydrogen. As the reported results, the carbon layer coated on the surface of catalyst decreased the light absorption, but enhanced the adsorption of CH_3OH.[34-39] An optimal amount of carbon coating on the surface of anatase TiO_2 was reported to be 3.5wt% for the best photo-activity for decomposition of methylene blue, owing to the improved dye adsorption.[39] In addition, the carbon coating layer could work as a barrier layer avoiding the oxidation of Ti^{3+} from H_2O or O_2,[19,20] enhancing the

stability of Ti^{3+} in TiO_2. It is obvious that the difference in ability of hydrogen generation for the five anatase samples under visible light irradiation mainly originated from the different concentrations of bulk Ti^{3+}, which could narrow the band gap for more visible light absorption by inserting an impurity level below the conduction band of TiO_2, and the different stability must reflect the different protection ability of the surface carbon layers.

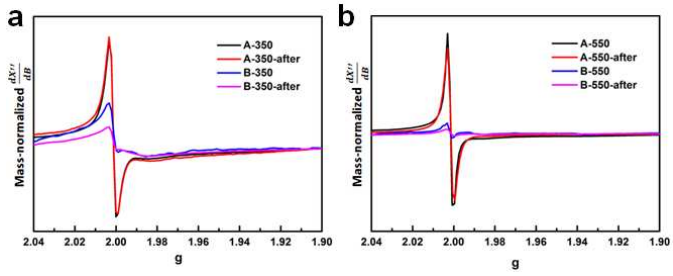

Fig.7 Normalized EPR spectra of samples A-350, B-350 (a) and A-550, B-550 (b) before and after 12 h visible light irradiation.

The excellent stability of photoactivity for the as-prepared carbon layer coated Ti^{3+}-doped anatase TiO_2 was also demonstrated by 36 h light irradiation (Fig.S5 of ESI†), which was a direct evidence to reflect the high stability of sample A-350 during the photoreaction. To confirm the stability of Ti^{3+} in sample A-350, the qualitative EPR analysis was carried out to evaluate the concentrations of surface oxygen vacancies and bulk Ti^{3+} of the as-prepared samples before and after photocatalytic hydrogen generation reaction,[10,18] as shown in Fig.7. Indeed, both of the samples B-350 and B-550 without carbon coating layer exhibited the obvious decrease in EPR signal for both of surface oxygen vacancies and bulk Ti^{3+} after 12 h photo-reaction. No visible difference in EPR peak intensity was observed for sample A-350 with carbon coating layer before and after photo-induced hydrogen production reaction, demonstrating that the carbon coating layer can stabilize the surface oxygen vacancies and bulk Ti^{3+} even if the carbon coating layer is as thin as 1 nm (for sample A-550) .

Usually, the Ti^{3+} defect and oxygen vacancy coexisted in the TiO_2 due to the thermodynamics requirement and charge balance for stabilization of such defects. Exposing the TiO_2 with bulk Ti^{3+} defects into the oxygen-rich environment, bulk Ti^{3+} excess charge can easily be withdrawn by the surface oxygen adsorbates, which could be transported from the surface to the bulk *via* gradually filling the bulk oxygen vacancies.[40, 41] In our case, the carbon coating layer as a barrier layer avoided directly exposing the surface of Ti^{3+}-doped TiO_2 into the methanol containing aqueous solution, thus suppressing the oxidation of surface oxygen vacancies and bulk Ti^{3+}.

Conclusions

In summary, the stable carbon coated Ti^{3+}-doped anatase TiO_2 nanocrystals were prepared by direct hydrothermal hydrolysis of titanium isopropoxide. We found that isopropanol, the hydrolysis production of titanium isopropoxide, could not only reduce the Ti^{4+} to Ti^{3+}, but also be an organic carbon source adsorbed on the surface of the as-prepared nanocrystals. After the calcination treatment in Ar, a carbon layer formed by the carbonization of the surface organics, which was an effectively protective layer to avoid directly exposing the surface of Ti^{3+}-doped TiO_2 into oxygen-rich environment. Therefore, the carbon coated Ti^{3+}-doped TiO_2 exhibited excellent stability for photocatalytic hydrogen production under visible light irradiation. Our results demonstrated that the carbon coating is a simple method for developing the stable and efficient Ti^{3+}-doped TiO_2 photocatalyst.

Acknowledgments

This work is supported by the National Basic Research Program of China (2013CB632404 and 2011CB933303), the National Natural Science Foundation of China (11174129, 51272101 and 61377051), the Science and Technology Research Program of Jiangsu Province (BK20130053) and the State Key Laboratory of NBC Protection for Civilian. (No. SKLNBC2014-09).

Notes and references

[a] National Laboratory of Solid State Microstructures & Ecomaterials and Renewable Energy Research Center (ERERC) at Department of Physics, Nanjing University, Nanjing 210093, P.R.China, Email: yutao@nju.edu.cn

[b] College of Engineering and Applied Sciences, Nanjing University, 210093, P.R.China, Email: yscfei@nju.edu.cn

[c] Collaborative Innovation Center of Advanced Microstructures, Nanjing University, Nanjing 210093, P.R.China

[d] Jiangsu Key Laboratory for Nano Technology, Nanjing University, Nanjing 210093, P.R.China

†Electronic Supplementary Information (ESI) available: Details of experimental procedures, characterizations, and supporting images. See DOI: 10.1039/c000000x/

1. A. Fujishia and K. Honda, *Nature*, 1972, **238**, 37.
2. X. B. Chen and S. S. Mao, *Chem. Rev.*, 2007, **107**, 2891.
3. N. Serpone, *J. Phys. Chem. B*, 2006, **110**, 24287.
4. M. Grätzel, *Nature,* 2001, **414**, 328.
5. S. Hoang, S. P. Berglund, N. T. Hahn, A. J. Bard and C. B. Mullins, *J. Am. Chem. Soc.*, 2012, **134**, 3659.
6. M. Ni, M. K. H. Leung, D. Y. C. Leung and K. Sumathy, *Renew. Sust. Ener. Rev.,* 2007, **11**, 401.
7. M. V. Dozzi and E. Selli, *J. Photo. Photo. C: Photo. Rev.*, 2013, **14**, 13.
8. L. B. Xiong, J. L. Li, B. Yang and Y. Yu, *J. Nanomater.*, 2012, **2012**, 1.
9. J. Su, X. Zou and J. S. Chen, *RSC Advance,* 2014, **4**, 13979.
10. F. Zuo, L. Wang, T. Wu, Z. Zhang, D. Borchardt and P. Feng, *J. Am. Chem. Soc.*, 2010, **132**, 11856.
11. F. Zuo, L. Wang and P. Feng, *Int. J. Hydr. Energy*, 2014, **39**, 711.
12. C. Mao, F. Zuo, Y. Hou, X. Bu and P. Feng, *Angew. Chem. Int. Ed.*, 2014, **53**, 10485.
13. J. Huo, Y. Hu, H. Jiang and C. Li, *Nanoscale*, 2014, **6**, 9078.
14. W. Fang, M. Xing and J. Zhang, *Appl. Cata. B: Environ.*, 2014, **160**, 240.
15. M. Xing, W. Fang, M. Nasir, Y. Ma, J. Zhang and M. Anpo, *J. Cata.*, 2013, **297**, 236.
16. A. Ookubo, E. Kanezaki and K. Ooi, *Langmuir*, 1990, 6, 206.
17. H. Zhang, Y. Zhao, S. Chen, B. Yu, J. Xu, H. Xu, L. Hao and Z. Liu, *J. Mater. Chem. A*, 2013, **1**, 6138.
18. Q. Zhu, Y. Peng, L. Lin, C. M. Fan, G. Q. Gao, R. X. Wang and A. W. Xu, *J. Mater. Chem. A*, 2014, **2**, 4429.

19. Y. Hu, X. Gao, L. Yu, Y. Wang, J. Ning, S. Xu and X. W. Lou, *Angew. Chem.Int. Ed.*, 2013, **52**, 5636.
20. J. Zhou, X. Zhang, W. Mu, Y. Deng, T. Lin, W. Song and L. Yu, *Micro. Meso. Mater.,* 2015, **204**, 115.
21. M. Inagaki, Y. Okada, H. Miura, H. Konno, *Carbon*, 1999, **37**, 329.
22. M. Inagaki, F. Kojin, B. Tryba and M. Toyoda, *Carbon*, 2005, **43**, 1652.
23. J. Y. Zhang, J. J. Wang, Z. Y. Zhao, T. Yu, J. Y. Feng, Y. J. Yuan, Z. K. Tang, Y. H. Liu, Z. S. Li and Z. G. Zou, *Phys. Chem. Chem. Phys.,* 2012, **14**, 4763.
24. B. Tryba, T. Tsumura, M. Janus, A. W. Morawski and M. Inagaki, *Appl. Cata. B: Environ.*, 2004, **50**, 177.
25. S. Pal, A. M. Laera, A. Licciulli, M. Catalano and A. Taurino, *Ind. Eng. Chem. Res.*, 2014, **53**, 7931.
26. H. W. Tien, Y. L. Huang, S. Y. Yang, J. Y. Wang and C. C. M. Ma, *Carbon*, 2011, **49**, 1550.
27. C. I. Oprea, P. Panait, J. Lungu, D. Stamate, A. Dumbravă, F. Cimpoesu and M. A. Gîrţu, Int. J. Photoenergy, 2013, 2013, 1.
28. B. Jiang, H. Yin, T. Jiang, Y. Jiang, H. Feng, K. Chen, W. Zhou and Y. Wada, Mater. Chem. and Phys., 2006, 98, 231
29. X. Liu, H. Xu, L. R. Grabstanowicz, S. Gao, Z. Lou, W. Wang, B. Huang, Y. Dai and T. Xu, *Cata. Today*, 2014, **225**, 80.
30. H. Liu, T. M. Ma, X. Z. Li, W. Z. Li, M. Wu and X. H. Bao, *Chemosphere*, 2003, **50**, 39.
31. D. Kulkarni and I. E. Wachs, *Appl. Cata. A: General*, 2002, **237**, 121.
32. H. S. Jung, H. Shin, J. R. Kim, J. Y. Kim, K. S. Kong and J. K. Lee, *Langmuir*, 2004, **20**, 11732.
33. H. Yu, S. Yan, Z. Li, T. Yu and Z. Zou, *Int. J. Hydr. Energy*, 2012, **37**, 12120.
34. R. Leary and A. Westwood, *Carbon*, 2011, **49**, 741.
35. T. Tsumura, N. Kojitani, I. Izumi, N. Iwashita, M. Toyoda and M. Inagaki, *J. Mater. Chem.*, 2002, **12**, 1391.
36. B. Tryba, T. Tsumura, M. Janus, A. W. Morawski and M. Inagaki, *Appl. Cata. B: Environ.*, 2004, **50**, 177.
37. F. Kojin, M. Mori, Y. Noda and M. Inagaki, *Appl. Cata. B: Environ.*, 2008, **78**, 202.
38. M. Inagaki, F. Kojin, B. Tryba and M. Toyoda, *Carbon*, 2005, **43**, 1652.
39. B. Tryba, A. W. Morawski, T. Tsumura, M. Toyoda and M. Inagaki, *J. Photochem. Photobiol. A: Chem.*, 2004, **167**, 127.
40. G. Lu, A. Linsebigler and J. T. Yates Jr., *J. Phys. Chem.*, 1994, **98**, 11733.
41. E. Lira, S. Wendt, P. Huo, J. O. Hansen, R. Streber, S. Porsgaard, Y. Wei, R. Bechstein, E. Laegsgaard and F. Besenbacher, *J. Am. Chem. Soc.*, 2011, **133**, 6529.
42. C. Wang, X. Zhang, C. Shao, Y. Zhang, J. Yang, P. Sun, X. Liu, H. Liu, Y. Liu, T. Xie and D. Wang, *J. Colloid Interface Sci.*, 2011, **363**, 157.
43. Y. Zhang, H. Gan and G. Zhang, *Chem. Eng. J.*, 2011, **172**, 936.